Extraction of Wind Direction Spreading Factor From Broad-Beam High-Frequency Surface Wave Radar Data

Chuan Li, Xiongbin Wu, Xianchang Yue, Lan Zhang, Jianfei Liu, Miao Li, Heng Zhou, and Bin Wan

***Abstract*— The spreading factor is considered as a key parameter that controls the concentration of the directional distribution of the wave energy. It has been confirmed by many scholars that there is a certain relationship between spreading factor and sea surface wind. In the application of high frequency surface wave radar (HFSWR), spreading factor is extracted from the ratio (R_B) of power spectrum density (PSD) of positive (P_B^+) and negative (P_B^-) Bragg peaks. To extract accurate spreading factor, the premise is that the PSD of detection unit is as little as possible affected by the adjacent detection units. For narrow-beam radar, digital beamforming (DBF) is easy to meet requirements. But for broad-beam radar, it is very difficult. In this paper, a new scheme is proposed to extract spreading factor from broad-beam HFSWR data with the MUSIC-APES algorithm. Different from spatial filtering by DBF, MUSIC-APES directly estimates the azimuth of positive or negative Bragg waves and their echo amplitudes. For broad-beam radar, this scheme can still achieve high azimuth resolution and accurate amplitude estimation at the same time. It solves the biggest obstacle to extract the spreading factor from broad-beam HFSWR data. To verify the feasibility of this scheme, simulations and experiments are carried out to compare with DBF. The extraction accuracy is improved greatly. The results are very surprising. It shows that spreading factor and wind speed are highly relevant. This may be a new way to extract wind speed in the application of HFSWR.**

***Index Terms*— APES, broad-beam, high-frequency surface wave radar (HFSWR), multiple signal classification (MUSIC), spreading factor, wind speed.**

I. Introduction

SEA surface wind is a key parameter of ocean dynamics. The wind and the wind-generated wave interact to determine the spatiotemporal variations of sea state, which are described by wave spectrum. Over the past decades, several wave spectrum models have been developed [1]–[5]. Among these, the directional wave spectrum model, $\cos^s(\theta_w/2)$, developed by Longuet-Higgins *et al.* [3] has been widely used to represent the angular distribution of wave energy. The parameter s, called spreading factor, is introduced to stand for the concentration of the directional distribution of the wave energy.

Based on this model, Mitsuyasu *et al.* [6] studied the directional spectrum of ocean wave using typical wave data measured by buoy and obtained an idealized form of s in terms of both the sea surface wind speed and the fetch. Hasselmann *et al.* [7] also investigated the properties and parameterizations of the directional wave spectrum using the buoy observation data and gave a new sight about the relationship among s, the wind speed, fetch, and wave spectrum peak frequency. These pioneer works ensure that s correlates tightly with wind speed. This result provides an alternative way of wind inversion from the values of s.

High-frequency surface wave radar (HFSWR) is capable of measuring sea state with high spatiotemporal resolutions [8]–[10]. The extraction methods of currents have been very mature [11]–[13] and the measurement range of some HFSWR systems can reach more than 200 km depending on operational frequency [14], [15]. However, the extraction of wind speed still presents a variety of difficulties relative to the measurement of the current [16], [17]. The popular methods for wind speed extraction from the HFSWR data are largely divided into two categories. One is based on the assumption that the relative magnitude of the second-order echoes in the Doppler spectrum is a function of wind speed and wave height [18]–[22]. All of these methods are viable and the results are quite encouraging. The wind speed extraction in this category is directly influenced by the quality of the second-order echoes. The other category is to infer wind speed directly from the first-order peaks with a prior knowledge of the wind speed [23]–[28]. These methods significantly expanded the range coverage of wind speed. However, the approach to the experiment and the way in which the model was built were empirical or semiempirical. These difficulties warrant the further efforts on constructing a robust and viable method of wind speed extraction from HFSWR data with better performance.

The spreading factor s can be derived from the HFSWR sea echo data. Heron and Rose deduced the method to derive s [29]. It involves the ratio of spectral energy density of the two first-order spectral lines and the using of Longuet-Higgins directional wave spectrum model. The spreading factor s extracted from narrow-beam HFSWR sea echo data

Manuscript received November 8, 2016; revised April 13, 2017 and April 28, 2017; accepted May 5, 2017. This work was supported in part by the National 863 High Technology Project of China under Grant 2012AA0917, in part by the National Natural Science Foundation of China under Grant 61401316, and in part by the National Natural Science Foundation of China under Grant 41474128. *(Corresponding authors: Xiongbin Wu; Xianchang Yue.)*

The authors are with the School of Electronic Information, Wuhan University, Wuhan 430072, China, and also with the Collaborative Innovation Center of Geospatial Technology, Wuhan, China (e-mail: whu_friday@whu.edu.cn; xbwu@whu.edu.cn; yuexc@whu.edu.cn).

Color versions of one or more of the figures in this paper are available online at http://ieeexplore.ieee.org.

Digital Object Identifier 10.1109/TGRS.2017.2702394

has been reported in [29]–[31]. Tyler *et al.* [31] compared the s derived from HFSWR data with that derived from buoy data and analyzed the relationship between radar derived s and buoy wind speed. They dedicated to use radio scatter from ocean waves for remotely sensing surface wind [31]. These pioneering works encourage us to work on the extraction of wind speed from HFSWR data by employing the relationship between s and wind speed. Therefore, it is essential to derive the s with high accuracy from HFSWR data.

Radar coverage is divided into small units in a polar coordinate by range and bearing centered at radar station. Range of a radar cell can be obtained accurately from the echo's time delay. The problem lies in the accurate determination of bearing [32]. For a HFSWR employing phased antennas, very long receiving arrays are needed to acquire a satisfactory azimuth resolution by deploying digital beamforming (DBF) technique [33], [34]. It is usually difficult and costly to deploy the array along the seashore. Consequently, HFSWRs with small antenna array are widely adopted. These HFSWRs usually receive broad-beams with effective width greater than 15°. It means that if DBF technology is used to extract the wind fields in broad-beam HFSWR data, the inverted wind parameter in one radar cell is the mean wind information over a very large patch. The results are too rough and unreasonable.

The goal of this paper is to design a scheme to extract s from broad-beam HFSWR data using the method documented by Heron and Rose [29]. The key point in this method is the calculation of the energy ratio of the two first-order spectrum lines (known also as positive/negative Bragg peak in literatures). DBF technique is applied in the processing of narrow-beam HFSWR data to provide estimations of the direction of arrival (DOA) with good azimuth resolution and the energy of the two Bragg peaks with rather good accuracy. Therefore, two aspects have to be focused in the proposed s extraction scheme: 1) one is the DOA estimation of two Bragg peaks and 2) the other is the energy estimations of the two Bragg peaks. The alternative to beamforming for bearing estimation in HF radar is the direction finding (DF) techniques such as the multiple signal classification (MUSIC) algorithm. Direction finding techniques are widely used to estimate the DOA of surface current [32]. Compared with narrow-beam radar system, they are likely possible to achieve high azimuth resolution with broad-beam HF Radar system. To map the wind direction using compact collocated antennas by direction-finding techniques, Fernandez *et al.* [35] had tried to extend the surface current algorithms [11], [32] to provide the Bragg power ratio for the extracted bearing angles corresponding to the particular Doppler frequency bin (or radial velocity). The bearing of a single source can be estimated accurately using DF techniques, but they cannot provide good estimation to the echo energy amplitude of the single source [36]. So we are committed to finding a new algorithm to calculate the ratio of two Bragg peaks from broad-beam radar data. So far, MUSIC is a powerful DF algorithm, which is particularly well suited for application to HF radar sea echo, and amplitude and phase estimation (APES) technology is a very effective source energy estimation algorithm [37].

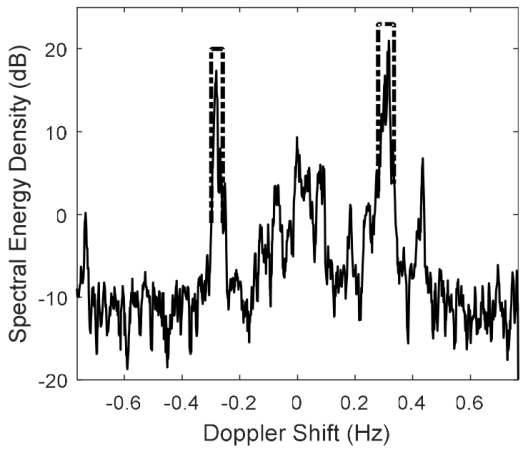

Fig. 1. Typical energy density spectrum from HFSWR. The dotted box is Bragg region.

Therefore, in the proposed scheme, we design to employ the MUSIC algorithm to estimate the DOA of two Bragg peaks and employ the APES algorithm to estimate the energy amplitude of the signal source with the estimated DOA.

The remainder of this paper is organized as follows. The scheme to extract the spreading factor from broad-beam HFSWR data will be introduced in Section II. Section III describes the application of MUSIC-APES method in HFSWR. Section IV presents the simulation results. Section V shows the experiment results and discussion. Conclusions are summarized in Section VI.

II. Scheme to Extract the Spreading Factor From Broad-Beam HFSWR Data

The method to derive the spreading factor s from narrow-beam HF radar has been documented by Heron and Rose [29] in detail. In this paper, we extend this method to a broad-beam HFSWR system.

A. Theoretical Model

In the absence of surface current, the theoretical formulation for the first-order backscatter cross section has been given in [38]. The current represents a transport of the water mass. It attaches its speed on the ocean waves. So the two Bragg peak will be shifted by a small amount proportional to the radial component of current velocity [8]. So, if the scattering patch has a net drift with a constant velocity $\boldsymbol{v}$, the first-order backscatter cross section per unit area per unit frequency interval σ_1 can be written as

$$\sigma_1(\omega) = 2^6 \pi k_0^4 \sum_{m=\pm 1} S(-2m\mathbf{k_0})\delta(\omega - m\omega_B - 2\mathbf{k_0}\boldsymbol{v}) \quad (1)$$

where ω is the Doppler frequency, $\mathbf{k_0}$ is the radar wavenumber, $S(\mathbf{k})$ is the directional wave spectrum, $m = \pm 1$ indicates the various positive and negative portions of the Bragg peaks, and $\omega_B = \sqrt{2gk_0}$ is the Bragg frequency shift (assuming the deep water dispersion equation holds for sea-surface gravity waves).

Equation (1) shows that the scattered waves are Doppler shifted from the first-order Bragg frequency by a $2\mathbf{k_0}\boldsymbol{v}$ offset. Fig. 1 shows a typical energy density spectrum at range bin r

from a receiving antenna. The received echoes are from all the scattering patches in the rth range bin. The current velocity in each patch is usually different, which broadens the Bragg peaks. The dotted box in Fig. 1 is called Bragg region. The method to determine the width of the box (i.e., the limits of the first-order Bragg region) is discussed in detail in [20]. For a broad-beam HFSWR, the MUSIC DF algorithm processes each spectral point where Bragg energy is detected in the doppler spectrum of the received signal, and determines the direction toward the patches of the ocean surface that are reflecting the radar signal at that Doppler shift [12]. And then, we employ APES amplitude determination algorithm to estimate the echo power backscattered from each patch.

We denote the echo power backscattered from each patch with the DOA φ and range r as $P_B^{\pm}(r,\varphi)$, the sign $\pm$ represents that the Bragg wave is approaching/receding from the radar site. The map of $P_B^{\pm}(r,\varphi)$, derived directly from the HF radar echo data, is usually gappy in the observable range-azimuth cells of the radar. To calculate $R_B = P_B^{+}/P_B^{-}$ at each range-azimuth cell, the gaps in $P_B^{\pm}(r,\varphi)$ have to be constructed in advance using interpolation method. The relationship between R_B and wind information discussed in [29] is as follows:

$$R_B = \tan^s(|\theta_0 - \theta_w|/2) \tag{2}$$

where θ_0 is the azimuth of the radar beam, θ_w is the azimuth of the wind vector, and s is the spreading factor to be extracted. The spreading factor is then

$$s = \ln(R_B)/\ln(\tan(|\theta_0 - \theta_w|/2)). \tag{3}$$

Heron and Rose [29] pointed out that using different radar beam azimuths to observe corresponding ratios R_B, θ_w, and s can be estimated jointly. The ambiguity of wind direction can also be resolved [29]. For the broad-beam HF radar, the different radar beam azimuth θ_0 values can be replaced by simultaneous radar observations of an ocean patch from two independent look angles.

B. Procedure to Extract s

The main purpose of this paper is to use the model formulated above to derive the map of spreading factor s on the common area simultaneously observed by broad-beam HF radars at two sites. The details of this method have these steps.

1) Determine the limits of the two Bragg regions in the Doppler spectrum as shown in Fig. 1 at the rth range cell.
2) Scan each spectral point contained in the Bragg regions, find out all the directions (φ) toward the patches with the same radial velocity (i.e., Doppler shifted frequency), and then estimate the echo power $P_B^{\pm}(r,\varphi)$ backscattered from each patch using the MUSIC-APES algorithm.
3) Repeat steps 1 and 2 from the first range bin to the end in the observable area of the radar.
4) Categorize the obtained $P_B^{\pm}(r,\varphi)$ into, $P_B^{+}(r,\varphi)$, the positive Bragg region and $P_B^{-}(r,\varphi)$, the negative Bragg region. Construct the energy density at the gap points of either group by polynomial interpolation.
5) Calculate R_B at each range-azimuth cell.
6) Using the HF radar data at the other site, repeat steps 1–5 and derive the map of R_B on the area observed by the second radar.
7) Substitute the R_B and θ_0 determined by the two radars, respectively, into (3) to estimate the spreading factor s and the wind direction θ_w at each range-azimuth cell in the common area observed by the two radars.

III. MUSIC-APES Approach

A MUSIC-APES algorithm is developed to determine the DOA and estimate the energy density $P_B^{\pm}(r,\varphi)$ of each patch of the ocean surface, which are reflecting the radar signal at step 2) of the scheme. The MUSIC algorithm is capable of estimating the DOAs of the signal sources with high azimuth resolution. In case that the DOA of a signal source is obtained, the APES algorithm can yield good amplitude estimates of the signal source.

A. Introduction of Array Signal Model and APES Algorithm

Consider a HFSWR radar system with a uniformly linear array (ULA). There are M omnidirectional antennas spaced by d ($d = \lambda/2$, λ is the radar wavelength). Assuming that there are K narrow-band sources with azimuth angles θ_k ($k = 1, 2, \ldots, K$) respect to the normal of the receiving array, respectively. They reflect the signals back to the radar receiver. The discrete-time signal received by the mth receiving antenna $x_m(i)$ is as follows:

$$x_m(i) = \sum_{k=1}^{K} e^{j(m-1)\omega_k}\beta(\theta_k, i) + \epsilon_m(i), \quad i = 1, \ldots, I \tag{4}$$

where $e^{j(m-1)\omega_k}$ is the array response of the mth receiving antenna to the signal from θ_k, $\omega_k = 2\pi d sin(\theta_k)/\lambda$ is the spatial angle frequency, $\beta(\theta_k, i)$ is the complex signal amplitude of the signal from θ_k in the ith sample, $\epsilon_m(i)$ denotes the interference-plus-noise term, and I denotes the number of samples.

Let $X(i)$ denote the signal matrix of the output of the M receiving arrays in the ith sample. It could be written as follows:

$$X(i) = A\boldsymbol{\beta}(i) + \boldsymbol{\epsilon}(i), \quad i = 1, \ldots, I \tag{5}$$

where

$$A = [\mathbf{a}_M(\omega_1), \mathbf{a}_M(\omega_2), \ldots, \mathbf{a}_M(\omega_K)] \tag{6}$$

$$\mathbf{a}_M(\omega_k) = [1, e^{j\omega_k}, \ldots, e^{j(M-1)\omega_k}]^T \tag{7}$$

$$\boldsymbol{\beta}(i) = [\beta(\theta_1, i), \beta(\theta_2, i), \ldots, \beta(\theta_K, i)]^T \tag{8}$$

$$\boldsymbol{\epsilon}(i) = [\epsilon_1(i), \epsilon_2(i), \ldots, \epsilon_M(i)]^T \tag{9}$$

where $(.)^T$ denotes the transpose. Let $(.)^c$ and $(.)^H$ denote the complex conjugate and the conjugate transpose, respectively.

The APES algorithm is applied to the above signal model to estimate the energy density magnitude of the signal scattered by a target with the azimuth angle θ. Here, we briefly review the APES algorithm. First, restructure $X(i)$ into a $N \times L$ Hankel-Matrix Z in a forward snapshot manner

$$Z = [z_0, z_1, \ldots, z_{L-1}] \tag{10}$$

and

$$z_l = [x_l(i), x_{l+1}(i), \ldots, x_{l+N-1}(i)]^T \tag{11}$$

where $l = 0, 1, \ldots, L-1$ and $L = M - N + 1$. z_l is N overlapping forward snapshot vectors of the data $X(i)$ and $x_l(i)$ is the lth element of $X(i)$. The Hankel-Matrix $\widetilde{Z}$ in the backward snapshot manner can be obtained from Z

$$\widetilde{Z} = J_N Z^c J_L \tag{12}$$

where J_N and J_L denote the exchange matrixes whose elements are zero except that the antidiagonal elements are one.

By following [37], the APES algorithm chooses filter $h \in N \times 1$ and complex amplitude $\beta(\theta, i)$ as joint minimizers of the following criterion:

$$\begin{aligned} \min_{h,\beta} \big(&\|h^H Z - \beta(\theta, i)\mathbf{a}_L^T(\omega)\|^2 \\ &+ \|h^H \widetilde{Z} - \beta^c(\theta, i)e^{-j(M-1)\omega}\mathbf{a}_L^T(\omega)\|^2 \big) \\ \text{s.t. } & h^H \mathbf{a}_N(\omega) = 1. \end{aligned} \tag{13}$$

Minimize the cost function in (13) with respect to $\beta(\theta, i)$ yields

$$\beta_{\text{APES}}(\theta, i) = \frac{\mathbf{a}_N^H(\omega) Q^{-1} \mu}{\mathbf{a}_N^H(\omega) Q^{-1} \mathbf{a}_N} \tag{14}$$

where $\mu = (1/L) Z \mathbf{a}_L(\omega)$, $\widetilde{\mu} = (1/L)\widetilde{Z}\mathbf{a}_L(\omega)$, and $Q = ZZ^H - \mu\mu^H + \widetilde{Z}\widetilde{Z}^H - \widetilde{\mu}\widetilde{\mu}^H$.

We perform the estimation of $\beta_{\text{APES}}(\theta, i)$ I times, and average them to get the amplitude $\beta_{\text{APES}}(\theta)$ in this period.

B. Applying MUSIC-APES Approach to HFSWR Data

This part describes in detail step 2) of the proposed scheme listed in Section II. MUSIC-APES approach processes each spectral point in Bragg peak box. The sample series in a spectral point is obtained using short-time Fourier transform (STFT).

Assume that the number of the antenna in the receiving ULA is 8. For the mth ($m = 1, \ldots, 8$) antenna, we choose a 1024 sequential echo records as a run. We set the parameters of STFT as the width of the window is 512 and the stepwise is 32. A time-frequency matrix with a size of 17×512 is obtained after applying STFT to the run. At a given spectral point in Bragg region, the corresponding column vector in the matrix is extracted out as the sample series, which equals to $x_m(i)$ ($i = 1, \ldots, 17$) in (4). The corresponding $X(i)$ is obtained then. The DOA and amplitude of echo power from each patch are estimated by the MUSIC-APES approach.

IV. Simulation

A. Simulation on MUSIC-APES Approach

To evaluate the performance of the proposed MUSIC-APES approach, we conduct simulations on determining the DOA of each signal sources and estimating their power spectrum density (PSD). The data is assumed to be collected by a HFSWR system with 8 receiving antenna in a ULA. The space d between adjacent antennas equals to half-wavelength λ. A linear frequency modulated interrupted continuous wave signal is transmitted at a fixed frequency of 7.8 MHz. The system parameters in simulation are the same as that of the radar used in the field experiment.

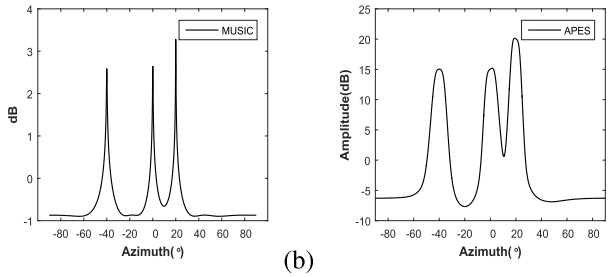

Fig. 2. Spatial spectral estimates, when $\theta_1 = -40°$, $\beta_1 = 15$ dB; $\theta_2 = 0°$, $\beta_2 = 15$ dB; and $\theta_3 = 20°$, $\beta_3 = 20$ dB. The SNR is 20 dB. (a) MUSIC. (b) APES.

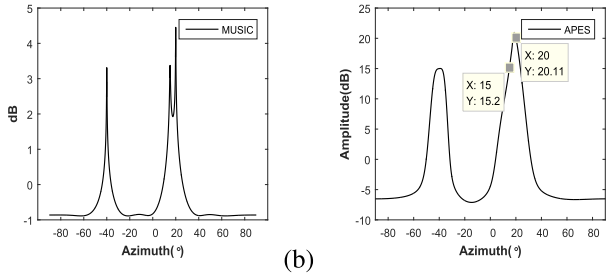

Fig. 3. Spatial spectral estimates, when $\theta_1 = -40°$, $\beta_1 = 15$ dB; $\theta_2 = 15°$, $\beta_2 = 15$ dB; and $\theta_3 = 20°$, $\beta_3 = 20$ dB. The SNR is 20 dB. (a) MUSIC. (b) APES.

Case 1: Three targets locate at sites with the same range from the radar receiving array. The azimuth angles respect to the normal direction of receiving array of the radar are $\theta_1 = -40°$, $\theta_2 = 0°$, and $\theta_3 = 20°$, respectively. Set the decibel modulus of complex amplitudes $\beta(\theta_{1-3})$ to be 15, 15, and 20 dB, respectively. The radial velocities of all the 3 targets are set to be 2 m/s, which means that they have the same Doppler shift frequency. The signal-to-noise ratio (SNR) is set to be 20 dB at this range bin. The simulation results are shown in Fig. 2. Fig. 2(a) shows the spatial spectrum estimated by the MUSIC algorithm. Three peaks occur at the preset target locations. Fig. 2(b) presents the amplitude-frequency spectrum estimated by the APES algorithm. There are peaks around the presented azimuth angles of the three targets. The estimated amplitude agrees quite well with the presented value for each target, but the peak width is much wider than that of MUSIC estimation.

Case 2: We consider a more challenging example where $\theta_2 = 15°$, while all the other simulation parameters are the same to Case 1. Now the angle between the second and the third targets is 5°. As shown in Fig. 3(a), in this case, the MUSIC algorithm is still capable to give the well-resolved peaks around the targets' locations. On the other hand, Fig. 3(b) shows that the APES algorithm fails to resolve the two closely spaced targets at $\theta_2 = 15°$ and $\theta_3 = 20°$. However, the estimated amplitudes at the target locations are 15.0, 15.2, and 20.11 dB, respectively, which agree quite well with the presented values.

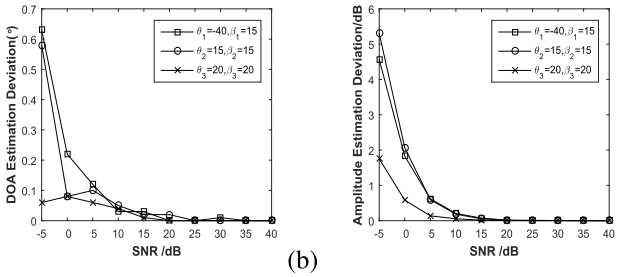

Fig. 4. Estimation deviation of MUSIC-APES versus SNR. (a) DOA estimation deviation. (b) Amplitude estimation deviation.

These results indicate we can reap the benefits of using the MUSIC and APES algorithms jointly. First, we use MUSIC method to estimate the DOA of the targets. And then, we use APES method to estimate the amplitudes at the azimuths estimated using the MUSIC method.

B. Sensitivity Analysis

A total of 500 Monte-Carlo simulations are conducted to test the sensitivity of the MUSIC-APES algorithm dependent on the SNR. The SNR is given randomly from -5 to 40 dB. All the other parameters of these simulations are the same to Case 2. The simulation results are statistically analyzed and plotted in Fig. 4. When SNR is larger than 10 dB, the deviation of the estimated DOA is less than 0.1° as shown in Fig. 4(a), meanwhile the deviation of the estimated amplitude decreases to be smaller than 0.5 dB, a precision larger than 95% (divided by the smallest preset amplitude of 15 dB) in Fig. 4(b). This indicates that the proposed MUSIC-APES algorithm performs excellent when the SNR is large enough. When SNR is -5 dB, the deviation in Fig. 4(b) is larger than 4.5 dB, i.e., the precision is less than 30%. This suggests that one should be caution in using the APES algorithm especially when SNR is not high.

C. Simulation on Extracting of Spreading Factor s

In this section, we perform the simulation to extract the spreading factor s from the sea surface wave echoes of HF radars at two sites. The first-order cross section of the surface wave is given by (1). The directional wave spectrum in (1) is approximated by the product of the JONSWAP frequency spectrum model and the angular distribution model, $A\cos^s(\theta/2)$, suggested by Longuet-Higgins *et al.* [3]. The surface current and wind field are assumed to be homogeneous in the area observed by the radars. The speed of the current is 1.2 m/s and the direction is 30° clockwise from the north. The wind speed at a place 10 m above the sea surface is set to be 10 m/s and the wind direction is set to be 45° clockwise from the north. Assuming two HFSWRs are fixed at sites labeled in Fig. 5. The parameters of the two radars are the same as that in simulation cases 1 and 2. The normal direction of the receiving array of antennas for both radars is 135° clockwise from the north. The backscattered radio wave from three patches (labeled by A, B, and C in Fig. 5) are used

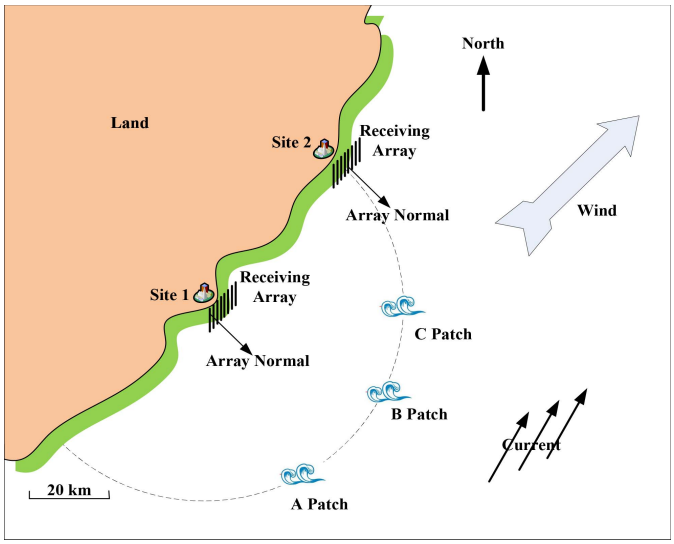

Fig. 5. Deployment diagram of simulation to extract spreading factor with two HFSWR sites.

TABLE I
SIMULATION RESULTS OF EXTRACTION OF SPREADING FACTOR WITH TWO HFSWR SITES

	Site 1 (dB)			Site 2 (dB)			s
	P_B^+	P_B^-	R_B	P_B^+	P_B^-	R_B	
A	-26.45	-31.28	4.83	-31.26	-49.78	18.52	4.5
B	-31.39	-25.51	-5.88	-24.89	-35.27	10.38	4.0
C	-36.61	-23.46	-13.15	-25.15	-30.27	5.12	3.5

for the extractions. A, B, and C patches are in the range-azimuth cells of $10-150.00°$ (the 10th range bin and at the direction of 150.00° from the north), $10-115.00°$, and $10-90.00°$, respectively, for the radar in Site 1, but are the cells of $17-183.43°$, $13-165.93°$, and $9-153.43°$, respectively, for the radar in Site 2. A range bin is equivalent to a distance of 5 km. The spreading factors s are set to be 4.2, 3.8, and 3.6, respectively, at patches A, B, and C. Using (3), according to the scheme outlined in Section II, the spreading factor s is extracted from the simulated sea echoes of these two radars from patches A, B, and C.

The extracted s values from the simulated sea-wave echoes are summarized in Table I. The relative error respect to the preset values of s is no larger than 7.5%. The magnitude of the relative error can be attributed to the SNR of sea-echoes, which degrades with distance [39]. The SNRs at patches A, B, and C are 18.53 dB for Site 1 and are 8.52 dB, 13.25 dB, and 20.81 dB, respectively, for Site 2. The noise added to the sea-echoes is Gaussian. Patch A is the farthest from the radar at Site 2, while patch C is the nearest. The distance from Site 2 to patch A is almost double that to patch C, which leads to the result that the relative error is 7.14% at patch A, while it is as small as 2.78% at patch C. The simulation result indicates that the proposed scheme is viable to extract the spreading factor s from the HFSWR data.

V. EXPERIMENT AND DISCUSSION

A. Introduction of Observation Network and Data

By deploying two HF radars and a fixed Buoy, a campaign was carried out by the SEA-STATE-Lab of Wuhan University

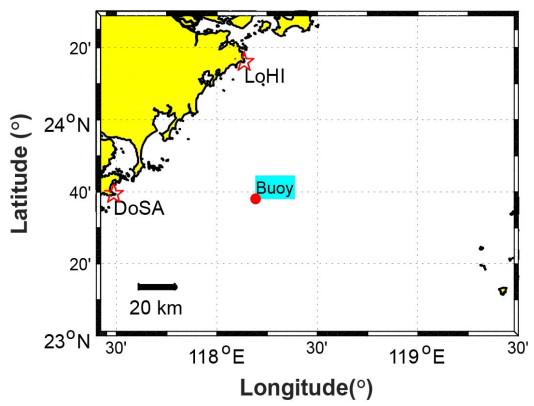

Fig. 6. Geographic diagram of observation network.

to measure the parameters of Chinese East sea surface state near Fujian province China during July 20, 2012 and July 31, 2012. The geographical sketch map of this campaign is shown in Fig. 6. The two red pentagrams represent the locations of the two radar sites (named by LoHI and DoSA, respectively), which is 94.7 km in distance from each other. The red solid circle represents the location of the Buoy, which is 70.6 and 72.5 km off the LoHI and DoSA sites, respectively. The sea surface wind vector at 10-m height (U_{10}) is measured by the fixed Buoy represented by red dot in Fig. 6. Wind speed measured by the buoy is at ranges of 0.5–60 m/s and wind direction is at ranges of 0–360°. The accuracy of wind speed is 5% of reading and the accuracy of wind direction is ±10°.

The OSMAR071 HFSWR, developed by Wuhan University, is fixed at the two sites. The parameters of the radar are the same as those used in the simulations in Section IV. The normal direction of receiving antenna array is 135° clockwise from the north for both radars. The half-power beamwidth of the receiving array is about 18°. The sea echo signals are collected up to 200-km offshore with a range resolution of 5 km and an integral time of 10 min. By applying the proposed scheme, the spread factor s is extracted from the data collected by these two radars.

B. Results

After the first three steps of the proposed scheme in Section II-B being performed, the DOA and the echo power from each patch are found out for all the frequency points included in the Bragg regions at all the observable ranges. Taking the data collected at 11:20 am on July 25, 2012, for example, the typical results at two selected spectral points are obtained and plotted in Figs. 7 and 8, respectively. The results are similar to the simulation cases 1 and 2. They are obtained from the Doppler spectrum at the 6th range bin of the radar data at DoSA site. The radial velocities corresponding to the selected spectral points are −34.46 and −5.75 cm/s, respectively, for Figs. 7 and 8. It is shown that there are three peaks resolved in both Fig. 7(a) and (b), respectively. The peaks in Fig. 7(a) locate at angles of 78°, 129°, and 187° clockwise from the north, respectively. However, the angles of the peaks in Fig. 7(b) are 90°, 125°, and 191° clockwise

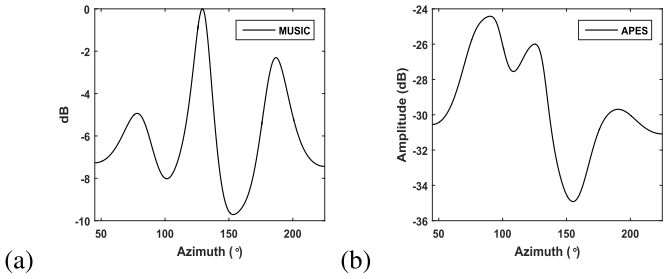

Fig. 7. Spatial spectral estimates. Here, the sea echo signal is from the 6th range cell of DoSA site (off the DoSA site about 30 km) at the time of 11:20 am on July 25, 2012. The corresponding radial current velocity of this spectral point in negative Bragg region is −34.46 cm/s. The azimuth refers to the north. (a) MUSIC. (b) APES.

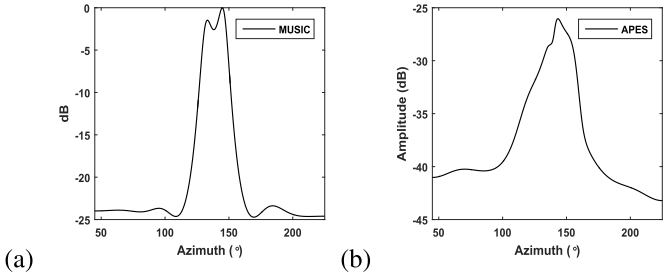

Fig. 8. Spatial spectral estimates. Here, the sea echo signal is from the 6th range cell of DoSA site (off the DoSA site about 30 km) at the time of 11:20 am on July 25, 2012. The corresponding radial current velocity of this spectral point in negative Bragg region is −5.75 cm/s. The azimuth refers to the north. (a) MUSIC. (b) APES.

from the north, respectively. Each peak envelope in Fig. 7(a) is obviously narrower than the corresponding peak envelope in Fig. 7(b).

In Fig. 8(a), there are two resolved peaks at 133° and 145° from the north, respectively. However, there is only one peak at 143° from the north in Fig. 8(b). This result is similar to the simulation case 2.

For each signal source, we take the peak angle estimated using the MUSIC algorithm, as shown in Fig. 7(a) or 8(a) as the DOA angle, and then sample the value estimated using the APES algorithm, as shown in Fig. 7(b) or 8(b), at the corresponding DOA angle as the energy density.

After step 4 of the proposed scheme, the estimated energy density $P_B^{\pm}(r,\varphi)$ distribution is obtained and plotted in Fig. 9. Both Fig. 9(a) and (b) shows that the magnitudes of the echo energy density decrease with increasing distance from the radar site. Which is consistent with the fact that the energy of radio waves transmitted by the radar will be attenuated as propagating over the sea surface [39]. The ratio of energy density R_B is obtained after step 5 of the proposed scheme. The resulted spatial distribution of R_B is shown on the left of Fig. 10. These steps are also conducted to the radar data at LoHI site, the resulted R_B is shown on the right of Fig. 10. The dark dashed curves overplotted on R_B denote the common area covered by these two radars. There are obvious differences between R_Bs of the two radars at same location. Take the location of the Buoy, for example, the values of R_B are 1.78 and 2.43, respectively, for DoSA and LoHI radars.

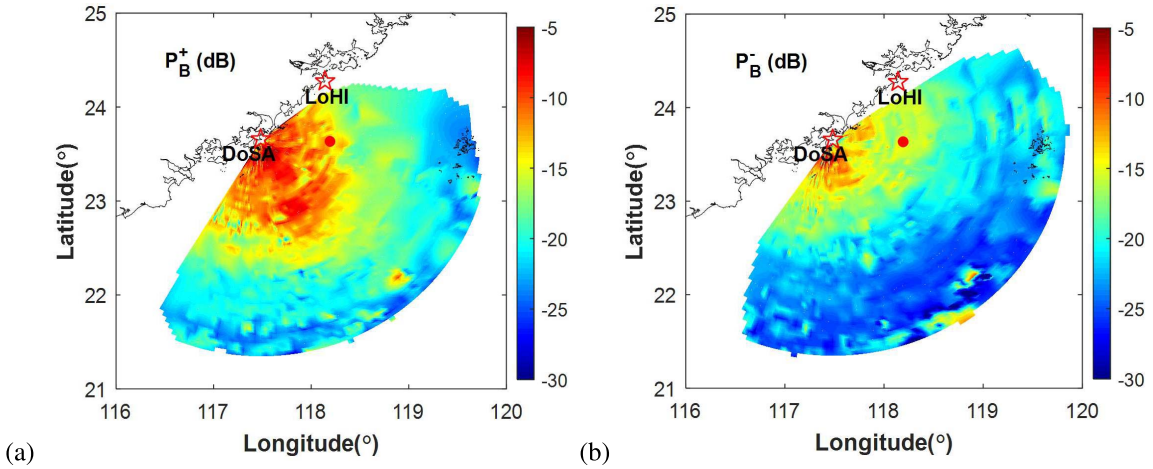

Fig. 9. Spatial distribution of P_B^+ and P_B^- at the time of 11:20 am on July 25, 2012 in DoSA site. (a) P_B^+: PSD of positive Bragg points. (b) P_B^-: PSD of negative Bragg points. The red solid circle represents the location of the Buoy.

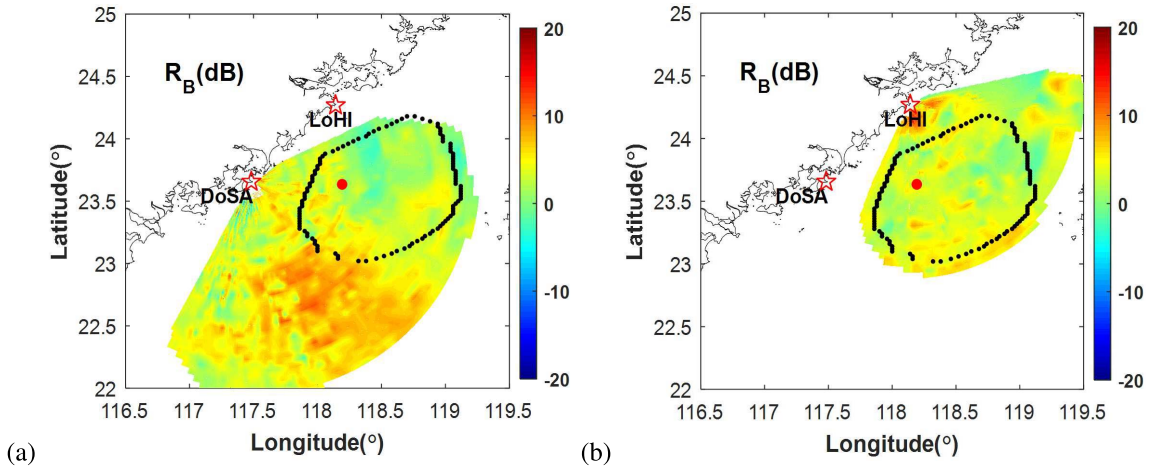

Fig. 10. Spatial distribution of R_B at the time of 11:20 am on July 25, 2012. (a) R_B in DoSA site. (b) R_B in LoHI site. The red solid circle represents the location of the Buoy.

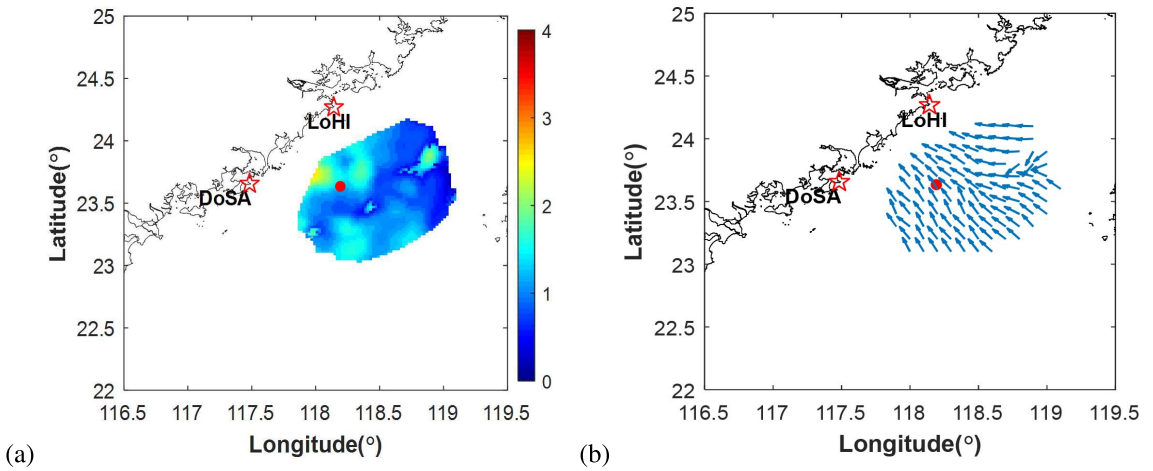

Fig. 11. Spatial distribution of spreading factor and wind direction at the time of 11:20 am on July 25 2012. (a) Spatial distribution of spreading factor. (b) Spatial distribution of wind direction. The red solid circle represents the location of the Buoy.

The extracted spreading factor s using (3) is plotted in Fig. 11(a). It is shown that s is not uniform in the area but exhibits some kind of spatial distribution. The values of s are smaller than 2 on most region at this moment, which is much smaller than the value of 4 usually adopted in the extraction of wind direction from HFSWR data [29], [35].

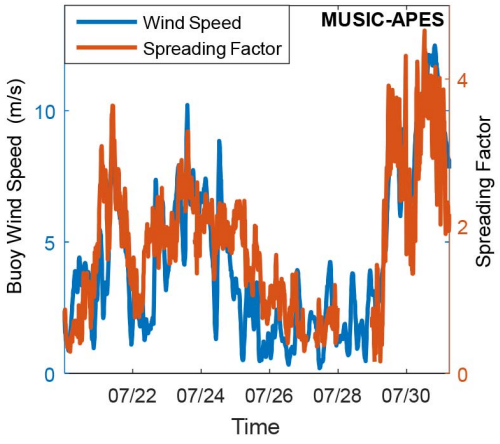

Fig. 12. Wind speed observed by buoy (marked as ink blue) versus spreading factor derived from HFSWR data at the Buoy site by MUSIC-APES (marked as orange red).

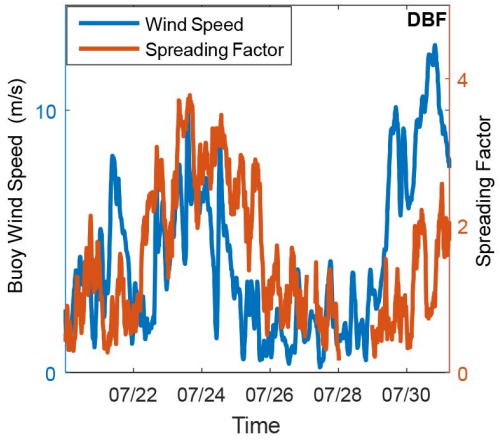

Fig. 13. Wind speed observed by buoy (marked as ink blue) versus spreading factor derived from HFSWR data at the Buoy site by DBF (marked as orange red).

The wind direction is also derived accompanying the extraction of s and is plotted in Fig. 11(b). There are two wind components in this area. The wind blows toward the coast in most of the area. But there is a gust of wind blows in the direction parallel to the coast from the north-east corner of the area. This wind turns left gradually and blows into the main wind component directing to the coast near the buoy location. We have compared the wind direction measured by the buoy with our result at Buoy site. The mean discrepancy between them is 22.66° for three days observation, while the root mean square (RMS) of the discrepancy is 36.89°. The mean discrepancy and RMS values are rather large, which can be attribute to the fact that the buoy is near the confluence of two components of the wind vector. The wind direction changes swiftly at the buoy site due to the alteration of the strength of the two wind components, but the wind direction estimated by the radar, which represents the bulk effect of the range-azimuth cell, changes much gentler.

The spreading factor s is assumed to be dependent on the wind speed [6], [31]. Therefore, we plot the s extracted at the buoy site and the wind speed measured by the buoy in Fig. 12 together. The amplitude of the wind speed is labeled on the left of y-axis, while s is labeled on the right. The simultaneous observations last for 11 days. The wind speeds in this period is not very big with the maximum no larger than 12 m/s. At the same time, the spreading factor s is less than four most of the time. The spreading factor s presents a similar trend to the wind speed in this period. The correlation coefficient between them is 0.83. This result provides strong support to the assumption of the dependence of s on the wind speed.

C. Discussion

In remote sensing of wind information by HFSWR, DBF techniques is a long-accepted method for isolating the scattering patch in bearing. Therefore, we replace the MUSIC-APES approaches in steps 1)–4) of the proposed method by DBF approach to estimate the energy density at each azimuth

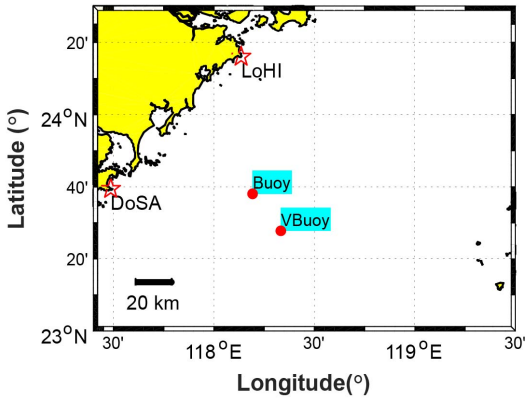

Fig. 14. Geographic diagram of the second observation network.

angles. For the radar deployed here, the beamwidth of the receiving array is about 18°. We use 36 lobes to scan the entire radar coverage. The interval of the adjacent lobes is 5°. The spreading factor is then extracted. Fig. 13 shows the temporal variations of s at the buoy site. Similar to Fig. 12, the wind speed observed by the buoy is also plotted for contrast. The estimated s still exhibits likely behavior to the wind speed. We calculated the correlation coefficient between s and the wind speed here, and got a value of 0.32, which is significantly smaller than 0.83, the value obtained from the data shown in Fig. 12. This comparison indicates that the estimations using the proposed method provide much stronger evidence to the assumption that s depends directly on the wind speed. The rational result gives an indirect validation to the accuracy of the proposed method in the estimation of s.

Another ocean state observation campaign has been conducted from January 29, 2013 to March 31, 2013. The HF radar observation network shown in Fig. 14 was the same as before. A buoy of the same type as before is fixed at another site (labeled as VBuoy), which is about 91km off the LoHI site and 90 km off the DoSA site. This experiment lasted for two months. The sea states in this period are more comprehensive, which provide a better chance to adequately

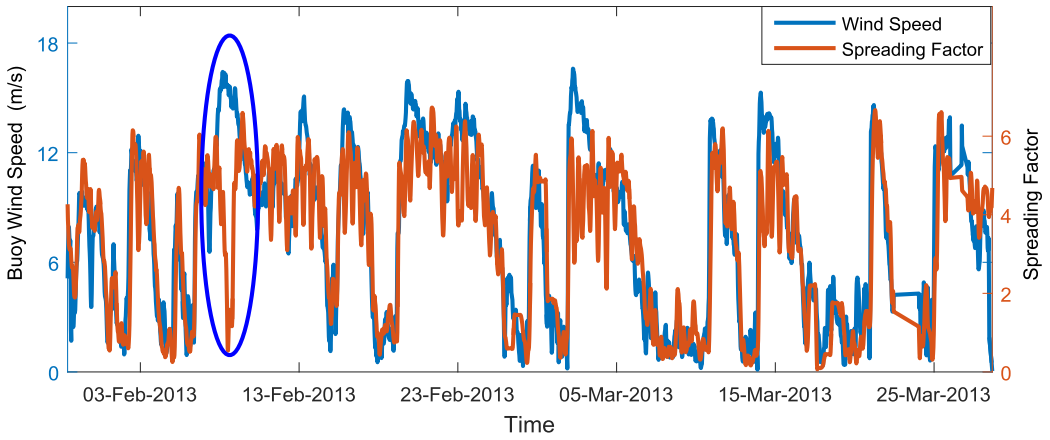

Fig. 15. Wind speed observed by buoy (marked as ink blue) versus spreading factor derived by HFSWR at VBuoy (marked as orange red). The observation time at VBuoy is from January 29, 2013 to March 31, 2013.

validate the s extraction by employing this proposed method.

We estimated the spreading factor s from the data observed simultaneously by the DoSA and LoHI radars in this period. The temporal variations of s at the VBuoy site are plotted in Fig. 15, together with the wind speed measured by the buoy. The similar temporal behavior between the wind speed and s is obviously exhibited in Fig. 15. This phenomenon agrees with that shown in Fig. 12. The correlation coefficient is as high as 0.91. This result presents further that the assumption of the dependence of s on the wind speed is rational and that the proposed method for s extraction is viable.

Comparing with Fig. 12, Fig. 15 shows stronger winds occur frequently in this period. The wind speeds are larger than 12 m/s in several days. The maximum reaches to about 16 m/s. The variations of s consist with that of wind speed when the wind speed is not larger than 12 m/s. However, s stops dancing with the wind and become chaotic when the wind speed is larger than 12 m/s. Furthermore, it is astonished to find that s oscillates almost 180° out of phase to the wind speed in the period circled by the blue curve in Fig. 15. The spreading factor s is defined to represent the concentration of the directional distribution of the wave energy. It is noted that the extracted s from the 1st spectra represents only the directional distribution of the Bragg wave, but not for each ocean wave [30]. The behaviors of s show that the directional distribution of wave energy at Bragg wavelength becomes increasingly concentrated with the increase of the wind speed. But when the wind speed reaches a certain value that is determined by fetch and duration (here the value is about 12 m/s), the concentration of the direction distribution turns to decrease or oscillate with the increase of wind speed. Now the Bragg wave reaches a saturated state and the wave energy begins to transfer to the lower frequency waves.

VI. Conclusion

In this paper, we propose and test a new method for extracting spreading factor s from broad-beam HF radar data. Both spreading factor s and wind direction, which are linked to the Bragg-resonant peaks, are estimated by employing data from two simultaneous HFSWR observations of an ocean patch from two independent look angles. We expand upon the method on the remote sensing of wind information using long receiving arrays and DBF techniques. The proposed method explicitly employs DF techniques applied to broad-beam configurations.

The novel approaches here include: 1) use of the sequential MUSIC DF algorithm and the APES amplitude determination algorithm and 2) use of spatial mapping of the gappy DF returns from each radar site prior to combining data from two sites.

The devised methodology is shown by detailed simulations and long period of field observations.

In simulation, we verify the performance of the MUSIC-APES algorithm. The MUSIC algorithm presents high bearing resolution. The APES algorithm is able to estimate the amplitudes rather accurately even for two undistinguished close targets in bearing. The percentage deviation of the estimation is less than 1.4%. We also evaluate the performance of extraction of s by the proposed method. For the three patches used in the simulation, the minimum deviation of s is only 2.78% in percentage and the maximum is 7.14%. The deviation depends on the distances of the patch from the two radar sites.

The field observations are conducted twice at different seasons. The one conducted in summer lasts 11 days, the other conducted in spring lasts more than two months. Buoys are employed to measure wind vector directly at two sites covered by both HF radars employed in these two observations.

For the first field experiment, we compare the spreading factor s estimated using MUSIC-APES approach and DBF approach. The correlation coefficients between them and the wind speed measured by the buoy are 0.83 and 0.32. For the second field experiment, the correlation coefficient between s extracted by our proposed method and the wind speed is 0.91. This strong correlation motivates further research into the possibility of estimating the wind speed from s extracted from the HFSWR data. In the field experiments, we also find that s becomes chaotic when the wind speed is high. These chaotic behaviors of s warrant further research

into the assumed spreading function shape at high wind speeds.

REFERENCES

[1] W. J. Pierson, Jr., and L. Moskowitz, "A proposed spectral form for fully developed wind seas based on the similarity theory of S. A. Kitaigorodskii," *J. Geophys. Res.*, vol. 69, no. 24, pp. 5181–5190, 1963.

[2] K. Hasselmann *et al.*, "Measurements of wind-wave growth and swell decay during the Joint North Sea Wave Project (JONSWAP)," *Dtsch. Hydrogr. Z*, vol. 12, no. 2, pp. 1–95, 1973.

[3] M. S. Longuet-Higgins, D. E. Cartwright, and N. D. Smith, *Observations of the Directional Spectrum of Sea Waves Using the Motions of a Floating Buoy*. Uppre Saddle River, NJ, USA: Prentice-Hall, 1963.

[4] M. A. Donelan, J. Hamilton, and W. H. Hui, "Directional spectra of wind-generated waves," *Philos. Trans. Roy. Soc. London A, Math. Phys. Sci.*, vol. 315, no. 1534, pp. 509–562, 1985.

[5] C. E. Long and D. T. Resio, "Wind wave spectral observations in Currituck Sound, North Carolina," *J. Geophys. Res., Oceans*, vol. 112, no. C5, pp. 392–394, 2007.

[6] H. Mitsuyasu *et al.*, "Observations of the directional spectrum of ocean waves using a cloverleaf buoy," *J. Phys. Oceanogr.*, vol. 5, no. 4, pp. 750–760, 1975.

[7] D. E. Hasselmann, M. Dunckel, and J. A. Ewing, "Free access directional wave spectra observed during JONSWAP 1973," *J. Phys. Oceanogr.*, vol. 10, no. 8, pp. 1264–1280, 1980.

[8] D. E. Barrick, M. W. Evans, and B. L. Weber, "Ocean surface currents mapped by radar," *Science*, vol. 198, no. 4313, pp. 138–144, 1977.

[9] M. L. Heron and P. Marrone, "Wind direction manifestation on HF ocean radar echoes," in *Proc. OCEANS*, 2010, pp. 1–6.

[10] L. R. Wyatt *et al.*, "Operational wave, current, and wind measurements with the pisces HF radar," *IEEE J. Ocean. Eng.*, vol. 31, no. 4, pp. 819–834, Oct. 2006.

[11] B. Lipa and D. Barrick, "Least-squares methods for the extraction of surface currents from CODAR crossed-loop data: Application at ARSLOE," *IEEE J. Ocean. Eng.*, vol. 8, no. 4, pp. 226–253, Oct. 1983.

[12] K. E. Laws, D. M. Fernandez, and J. D. Paduan, "Simulation-based evaluations of HF radar ocean current algorithms," *IEEE J. Ocean. Eng.*, vol. 25, no. 4, pp. 481–491, Oct. 2000.

[13] J. T. Kohut and S. M. Glenn, "Free access improving HF radar surface current measurements with measured antenna beam patterns," *J. Atmos. Ocean. Technol.*, vol. 20, no. 9, p. 1303, 2003.

[14] J. T. Kohut, H. J. Roarty, and S. M. Glenn, "Characterizing observed environmental variability with HF Doppler radar surface current mappers and acoustic Doppler current profilers: Environmental variability in the coastal ocean," *IEEE J. Ocean. Eng.*, vol. 31, no. 4, pp. 876–884, Oct. 2006.

[15] R. Gomez *et al.*, "Real-time quality control of current velocity data on individual grid cells in WERA HF radar," in *Proc. OCEANS*, 2014, pp. 1–7.

[16] B. J. Lipa and D. E. Barrick, "Extraction of sea state from HF radar sea echo: Mathematical theory and modeling," *Radio Sci.*, vol. 21, no. 1, pp. 81–100, 1986.

[17] W. Huang, S. Wu, E. Gill, B. Wen, and J. Hou, "HF radar wave and wind measurement over the Eastern China Sea," *IEEE Trans. Geosci. Remote Sens.*, vol. 40, no. 9, pp. 1950–1955, Sep. 2002.

[18] D. E. Barrick, "Remote sensing of sea state by radar," in *Remote Sensing of the Troposphere*, vol. 12, V. E. Derr, Ed., Washington, DC, USA: Printing Office, 1972.

[19] J. L. Ahearn, S. R. Curley, J. M. Headrick, and D. B. Trizna, "Tests of remote skywave measurement of ocean surface conditions," *Proc. IEEE*, vol. 62, no. 6, pp. 681–687, Jun. 1974.

[20] P. E. Dexter and S. Theodoridis, "Surface wind speed extraction from HF sky wave radar Doppler spectra," *Radio Sci.*, vol. 17, no. 3, pp. 643–652, 1982.

[21] D. E. Barrick, "Extraction of wave parameters from measured HF radar sea-echo Doppler spectra," *Radio Sci.*, vol. 12, no. 3, pp. 415–424, 1977.

[22] D. Green, E. Gill, and W. Huang, "An inversion method for extraction of wind speed from high-frequency ground-wave radar oceanic backscatter," *IEEE Trans. Geosci. Remote Sens.*, vol. 47, no. 10, pp. 3338–3346, Oct. 2009.

[23] R. H. Stewart and J. R. Barnum, "Radio measurements of oceanic winds at long ranges: An evaluation," *Radio Sci.*, vol. 10, no. 10, pp. 853–857, 1975.

[24] J. Maresca, Jr., and J. Barnum, "Measurement of oceanic wind speed from HF sea scatter by skywave radar," *IEEE J. Ocean. Eng.*, vol. 2, no. 1, pp. 132–136, Jan. 1977.

[25] J. F. Vesecky, J. A. Drake, K. Laws, F. L. Ludwig, C. C. Teague, and L. A. Meadows, "Using multifrequency HF radar to estimate ocean wind fields," in *Proc. IEEE Int. Geosci. Remote Sens. Symp.*, Sep. 2005, pp. 4769–4772.

[26] J. Drake, J. Vesecky, K. Laws, C. Teague, F. Ludwig, and J. Paduan, "Vector wind field measurements using multifrequency HF radar," in *Proc. IEEE/OES 7th Working Conf. Current Meas. Technol.*, Mar. 2003, pp. 88–91.

[27] W. Shen, K.-W. Gurgel, G. Voulgaris, T. Schlick, and D. Stammer, "Wind-speed inversion from HF radar first-order backscatter signal," *Ocean Dyn.*, vol. 62, no. 1, pp. 105–121, 2012.

[28] A. Kirincich, "Remote sensing of the surface wind field over the coastal ocean via direct calibration of HF radar backscatter power," *J. Atmos. Ocean. Technol.*, vol. 33, no. 7, pp. 1377–1392, 2016.

[29] M. L. Heron and R. Rose, "On the application of HF ocean radar to the observation of temporal and spatial changes in wind direction," *IEEE J. Ocean. Eng.*, vol. 11, no. 2, pp. 210–218, Apr. 1986.

[30] M. L. Heron, "Directional spreading of short wavelength fetch-limited wind waves," *J. Phys. Oceanogr.*, vol. 17, no. 2, pp. 281–285, 1987.

[31] G. L. Tyler, C. C. Teague, R. H. Stewart, A. M. Peterson, W. H. Munk, and J. W. Joy, "Wave directional spectra from synthetic aperture observations of radio scatter," *Deep Sea Res. Oceanogr. Abstracts*, vol. 21, no. 12, pp. 989–1016, 1974.

[32] D. E. Barrick and B. J. Lipa, "Evolution of bearing determination in HF current mapping radars," *Oceanography*, vol. 10, no. 2, pp. 72–75, 1997.

[33] M. L. Heron and N. R. Mclaren, "Groundwave HF ocean surface radar," in *Proc. Conf. Pacific Ocean Environ. Probing (PORSEC)*, vol. 1, Okinawa, 1992, pp. 71–75.

[34] S. Yang, H. Ke, X. Wu, J. Tian, and J. Hou, "HF radar ocean current algorithm based on MUSIC and the validation experiments," *IEEE J. Ocean. Eng.*, vol. 30, no. 3, pp. 601–618, Jul. 2005.

[35] D. M. Fernandez, H. C. Graber, J. D. Paduan, and D. E. Barrick, "Mapping wind directions with HF radar," *Oceanography*, vol. 10, no. 2, pp. 93–95, 1997.

[36] J. Li and P. Stoica, *MIMO Radar Signal Processing*. Hoboken, NJ, USA: Wiley, 2008.

[37] J. Li and P. Stoica, "An adaptive filtering approach to spectral estimation and SAR imaging," *IEEE Trans. Signal Process.*, vol. 44, no. 6, pp. 1469–1484, Jun. 1996.

[38] D. Barrick, "First-order theory and analysis of MF/HF/VHF scatter from the sea," *IEEE Trans. Antennas Propag.*, vol. 20, no. 1, pp. 2–10, Jan. 1972.

[39] P. Forget, P. Broche, and J. C. de Maistre, "Attenuation with distance and wind speed of HF surface waves over the ocean," *Radio Sci.*, vol. 17, no. 3, pp. 599–610, 1982.

Chuan Li received the B.S. and M.S. degrees from Wuhan University, Wuhan, China, in 2013 and 2015, respectively, where he is currently pursuing the Ph.D. degree with the School of Electronic Information.

His research interests include ocean wave parameter retrieval from ocean remote sensing by HF surface wave radar.

Xiongbin Wu received the B.Sc. degree in geophysics from Beijing University, Beijing, China, in 1990, and the Ph.D. degree in space physics from Wuhan University, Wuhan, China, in 1999.

Since 1994, he has been involved in high-frequency surface wave radar (HFSWR) and radio wave propagation studies. He is one of the original contributors to the development of the ocean state monitoring and analyzing radar series HFSWR. He is currently the Principal Investigator of the HFSWR Project in the National High-Tech Research and Development Program of China (863 program), in which an HF hybrid radar network had been built for the purpose of ocean dynamics surveillance in a wider area than the HFSWR covers. He is also a Professor of Radio Physics with the School of Electronic Information, Wuhan University. His research interests include HF/microwave radar remote sensing of ocean dynamics under high sea states and abnormal events, and ionospheric radio wave propagation.

Dr. Wu was a recipient of several awards from the China Ocean Engineering Society, the Ministry of Science and Technology of China, and the Ministry of Education of China.

Xianchang Yue received the B.S. and M.S. degrees in computational mathematics and the Ph.D. degree in space physics from Wuhan University, Wuhan, China, in 1996, 1999, and 2005, respectively.

Since 2005, he has been an Associate Professor with the Electronic Information School, Wuhan University. His current research interests include numerical simulation in atmospheric-oceanic dynamics, and ocean wind and wave retrieval from ocean remote sensing by high-frequency radar.

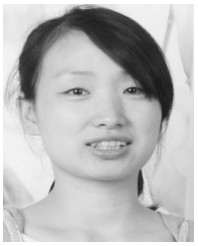

Lan Zhang received the B.Sc. degree in communication engineering, the M.S. degree in signal and information processing, and the Ph.D. degree in radio physics from Wuhan University, Wuhan, China, in 2004, 2006, and 2015, respectively.

Her research interests include the design of HF radar system and HF radar remote sensing of ocean dynamics.

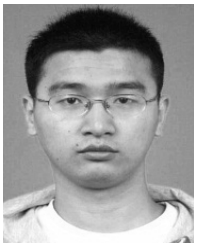

Jianfei Liu was born in Hubei, China, in 1989. He received the B.E. degree from Wuhan University, Wuhan, China, in 2012, where he is currently pursuing the Ph.D. degree with the School of Electronic Information.

He is currently a Visiting Ph.D. Student with the University of Colorado Boulder, Boulder, CO, USA, since 2015. His research interests include satellite oceanography and HF radar remote sensing.

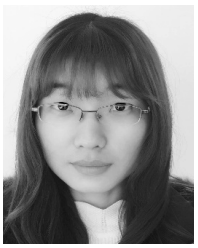

Miao Li was born in Hubei, China, in 1993. She received the B.E. degree from Xidian University, Xi'an, China, in 2014. She is currently pursuing the Ph.D. degree with the School of Electronic Information, Wuhan University, Wuhan, China.

She has been devoting herself to the high-frequency radar remote sensing research and sky-surface wave radar signal processing since 2014.

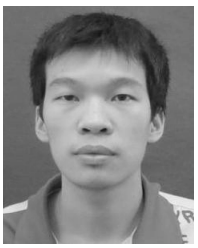

Heng Zhou was born in Hubei, China, in 1993. He received the B.S. degree from Wuhan University, Wuhan, China, in 2016, where he is currently pursuing the Ph.D. degree with the School of Electronic Information.

His research interests include high-frequency radar and obtaining ocean dynamic parameters from the sea echoes of HF radar.

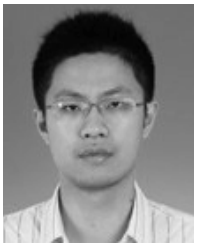

Bin Wan was born in Jiangxi, China, in 1984. He received the bachelor's degree in electronic information science and technology from East China Normal University, Shanghai, China, in 2005, and the master's degree in astronomical techniques and methods from the Shanghai Astronomical Observatory, Chinese Academy of Sciences, Shanghai, in 2010. He has been pursuing the Ph.D. degree in radio physics with Wuhan University, Wuhan, China, since 2015.

His research interests include high-frequency radar remote sensing.